Direct numerical simulation of a turbulent reacting jet

By B. J. Boersma

1. Motivation and objectives

Turbulent reacting jets are important in many engineering applications such as fuel injectors in diesel engines and in furnaces. Numerical simulations of such reacting jets are very useful in the design and optimization of these applications, mainly because physical experiments are very difficult to perform in the hostile environment in which these flows occur.

Traditional modeling approaches of turbulent reacting flows involve the solution of the Favre averaged Navier-Stokes equations, (see e.g. Gatski 1997), using simple two equation models such as the $k-\epsilon$ model or the more advanced Reynolds stress models. Due to the lack of experimental data for reacting flows and the uncertainty in the empirical constants in the turbulence models, the results of these simulation are questionable. A more advanced modeling approach is the large eddy simulation (LES) (see Ferziger 1996). In this technique only the small scales of motion are modeled and the large scales are solved explicitly on the computational grid. In the past, much effort has been put in the LES modeling of incompressible flows, and some reasonably good models are available (see e.g. Galperin & Orszag 1993). For compressible flows some models are available for the Favre averaged Navier-Stokes equations. It is not clear if these models are as good as the models for incompressible flows because there is only a limited amount of experimental data available, and the Favre averaging makes comparison with the experimental data difficult. Moreover, the chemical reactions also introduce many terms which have to be modeled, and until now there has been no reliable model available for this. Therefore, in this paper we will use direct numerical simulation (DNS), which does not use any model and in principle resolves every scale of motion. This method is inherently very expensive compared to all the methods described previously, but is also much more reliable. The generated database can then be used to validate LES subgrid models (Wall, Boersma & Moin 1999) and to investigate the influence of the chemical heat release on turbulent flow phenomena. In the past some DNS of reacting flows have been performed (see for instance Vervisch and Poinsot 1998). These simulations were restricted to very simple geometries such as plain mixing layers. As far as we know there is no DNS data available for reacting jets.

For the DNS of the jet flow we use basically the same code Boersma *et al.* (1997) and Lubbers *et al.* (1999) have used. This code has been extended with the low Mach number approximation as described by Najm *et al.* (1998). The motivation for the use of this approximation is that we are basically interested in flows with velocities which are small compared to the speed of sound. A solution of the full set of equations would place a too severe restriction on the timestep of the numerical scheme.

2. Governing equations and the low Mach number approximation

In this paper we study a flow in which the fluid velocity u is low compared to the acoustic velocity c. The dimensionless number formed by these two velocities, i.e. the Mach number $Ma = u/c$, will be small. If we would solve the full compressible equations numerically, the timestep of a numerical scheme would be proportional to $|u + c|^{-1}$. So the speed of sound would place a severe restriction on the time step of the numerical scheme while we expect that the effect of the acoustics on the flow will be small because of the low Mach number. Therefore it seems useful to eliminate the acoustic waves from the problem and try to retain the non constant properties, i.e. temperature dependent density and viscosity.

This can be done (following McMurtry *et al.*, 1986) by expanding all variables in the power series

$$f = f_0 + \gamma Ma^2 f_1 + (\gamma Ma^2)^2 f_2 + .., \tag{1}$$

where γMa^2 as a small parameter, f is flow variable, and γ the specific heat ratio.

The resulting non-dimensional equations for mass and momentum then read

$$\frac{\partial \rho}{\partial t} + \frac{\partial}{\partial x_i}\rho u_i = 0, \tag{2}$$

$$\frac{\partial \rho u_i}{\partial t} + \frac{\partial}{\partial x_i}\rho u_i u_j = -\frac{\partial}{\partial x_i}p_1 + \frac{\partial}{\partial x_i}\tau_{ij}, \tag{3}$$

where ρ is the density, u the velocity, p_1 the hydrodynamic pressure, and τ_{ij} the Newtonian stress tensor which is defined as

$$\tau_{ij} = \mu\left(\frac{\partial u_i}{\partial x_j} + \frac{\partial u_j}{\partial x_i} - \frac{2}{3}\delta_{ij}\frac{\partial u_i}{\partial x_i}\right), \tag{4}$$

where δ_{ij} is the Kronecker delta and μ is the dynamic viscosity.

The non-dimensional equation for the temperature T and chemical species Y_n read

$$\frac{\partial \rho T}{\partial t} + \frac{\partial}{\partial x_i}\rho u_i T = \frac{\partial}{\partial x_i}k_e\frac{\partial}{\partial x_i}T + h_p\dot{\omega}, \tag{5}$$

$$\frac{\partial \rho Y_n}{\partial t} + \frac{\partial}{\partial x_i}\rho u_i Y_n = \frac{\partial}{\partial x_i}k_c\frac{\partial}{\partial x_i}Y_n - \dot{\omega}, \tag{6}$$

where k_e, k_c are the thermal and chemical diffusivity, h_P the heat of formation, and $\dot{\omega}$ the reaction rate which will be specified later on. The equation of state

$$P_0 = \rho T, \tag{7}$$

relates the temperature and density to each other. In an open computational domain, we can assume that P_0 is spatially constant, and without loss of generality we can take P_0 equal to unity, so $\rho = 1/T$.

The viscosity and diffusivities in the transport equations are temperature dependent. For the viscosity we take the following simple law

$$\frac{\mu}{\mu_{ref}} = \left(\frac{T}{T_{ref}}\right)^{0.75}, \tag{8}$$

where μ_{ref} is the viscosity at the reference temperature T_{ref}. The diffusivities appearing in the transport equations are given by the temperature dependent viscosity divided by the Schmidt or Prandtl number. Both the Schmidt and Prandtl number are taken equal to 0.7.

Equation (5) can not be integrated in the form given previously because the time derivative of ρT is zero in the low Mach number approximation. Therefore, Eq. (5) has been rewritten, using the continuity Eq. (2), as

$$\frac{\partial T}{\partial t} + \frac{\partial}{\partial x_i} u_i T + T\frac{\partial u_i}{\partial x_i} = \frac{1}{\rho}\frac{\partial}{\partial x_i} k_e \frac{\partial}{\partial x_i} T + h_p \omega/\rho, \tag{9}$$

which is from a numerical point of view preferable over the advective form $\rho \partial T/\partial t + \rho u_i \partial T/\partial x_i$.

Numerical method

Recently, new high order compact finite difference schemes based on Pade approximations (see Lele 1992) have been developed for the DNS of turbulent flows. These schemes are relatively simple to implement and have a high accuracy for a large range of wavenumbers. However, the discretization given by these schemes is not fully conservative, in the sense that kinetic energy is not fully conserved for flows with low Mach numbers. In practice this means that the grid spacing should be so fine that all the scales of motion including the Kolmogorov scales are resolved; otherwise, the calculation becomes numerically unstable. Moin & Mahesh (1998) argue that it is not necessary to fully resolve the Kolmogorov scales in a DNS and that the cut-off should be somewhere close to the Taylor microscale. The schemes based on Pade approximations can not be used for such a simulation without a model for the unresolved scales (see Boersma & Lele 1999). Therefore, we use a low order method based on the method used by Harlow & Welch (1965), which is conservative.

The spatial derivatives in Eqs. (2), (3), (6), and (8) are calculated on a staggered spherical grid with the scalar fields located at the center of the grid cell and the velocity points at the sides of the grid cell. For a discussion about the use of the spherical grid instead of a cylindrical grid, we refer to Boersma *et al.* (1997). All terms in the momentum equations are discretized using second order central discretizations. The non-linear terms in the transport equation have been discretized by means of a flux corrected transport scheme (see Koren 1993). This scheme has been used to avoid negative scalar concentrations due to numerical dispersion errors. The continuity equation is satisfied with help of a pressure correction method. The resulting Poisson equation has been solved with a direct method.

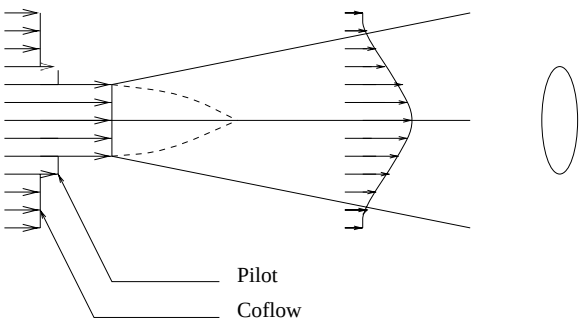

FIGURE 1. The geometry of the jet.

The time integration is very similar to the method used by Najm *et al.* (1998). The only difference between our method and the method used by Najm *et al.* (1998) is that we use the predictor corrector approach not only for the transport equations, but also for the momentum equations.

3. The jet geometry and chemistry

The geometry of the jet we study is shown in Fig. 1. The central fuel stream is surrounded by a small pilot stream (or pilot flame) which has a temperature which is nearly adiabatic ($T = 0.99T_b$, where T_b is the adiabatic temperature), which in turn is again surrounded by a cold stream with oxidizer. The velocity of the coflow is 10% of the orifice velocity, and the velocity of the pilot is 30% of the orifice velocity. The pilot will not have a large influence on the flow field because its momentum ρU_p^2 is small compared to the momentum of the jet ρU_j^2. For instance, for a heat release of five, the ratio of coflow momentum to orifice momentum is 0.018.

For the chemistry in the jet flow, we use a simple binary reaction

$$F + O \rightarrow 2P, \tag{16}$$

where F stands for the fuel, O for the oxidizer, and P for the product. The factor 2 has been included in the reaction to conserve mole fractions. The reaction rate is assumed to be given by the temperature dependent reaction rate (Arrhenius rate)

$$\dot{\omega} = \mathbf{A} \cdot [F][O] \exp[-K/RT], \tag{17}$$

where $\mathbf{A}$ is the so-called pre-exponential factor, $[F]$ and $[O]$ are the fuel and oxidizer concentrations, K the activation energy, and R the gas constant. In the simulations we use the following non-dimensional variant of the equation given above (see Chen *et al.* 1992):

$$\dot{\omega} = A\rho^2 Y_f Y_o \exp[-\beta[(1-\Theta)/(1-\alpha(1-\Theta))], \tag{18}$$

where Y_f and Y_o are the fuel and oxidizer concentrations (normalized between 0 and 1, β the Zeldovich number, $\Theta = (T - T_0)/(T_b - T_0)$, and $\alpha = (T_b - T_0)/T_b$ the heat release. The fuel and oxidizer concentrations are specified at the inflow plane. In the jet $Y_f = 1$ and $Y_o = 0$ in the coflow $Y_f = 0$, $Y_o = 1$, and in the

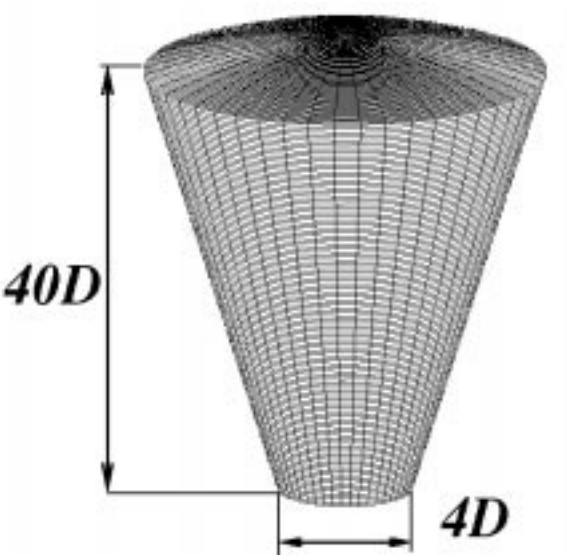

FIGURE 2. A typical computational grid.

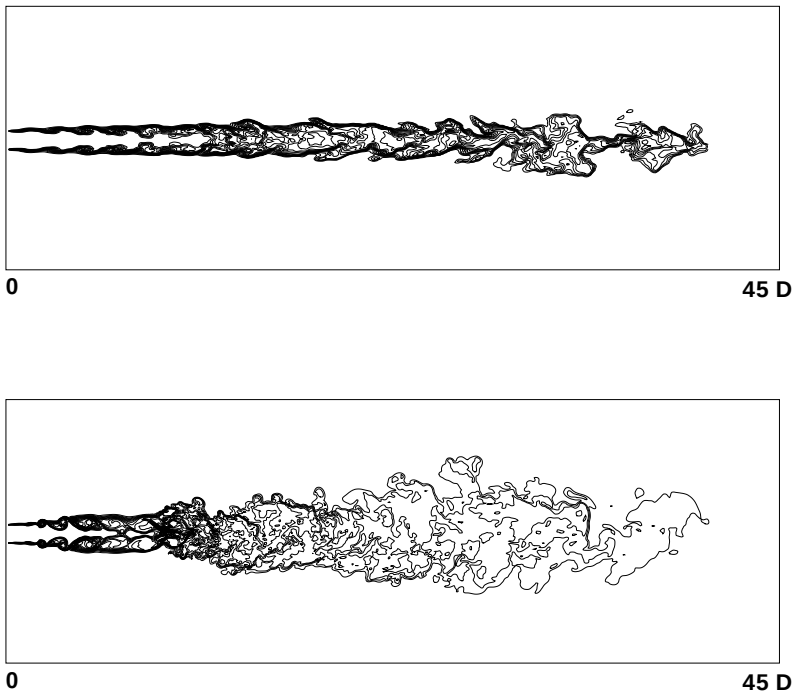

FIGURE 3. The distribution of the fuel in a reacting jet (top) and a non-reacting jet (bottom).

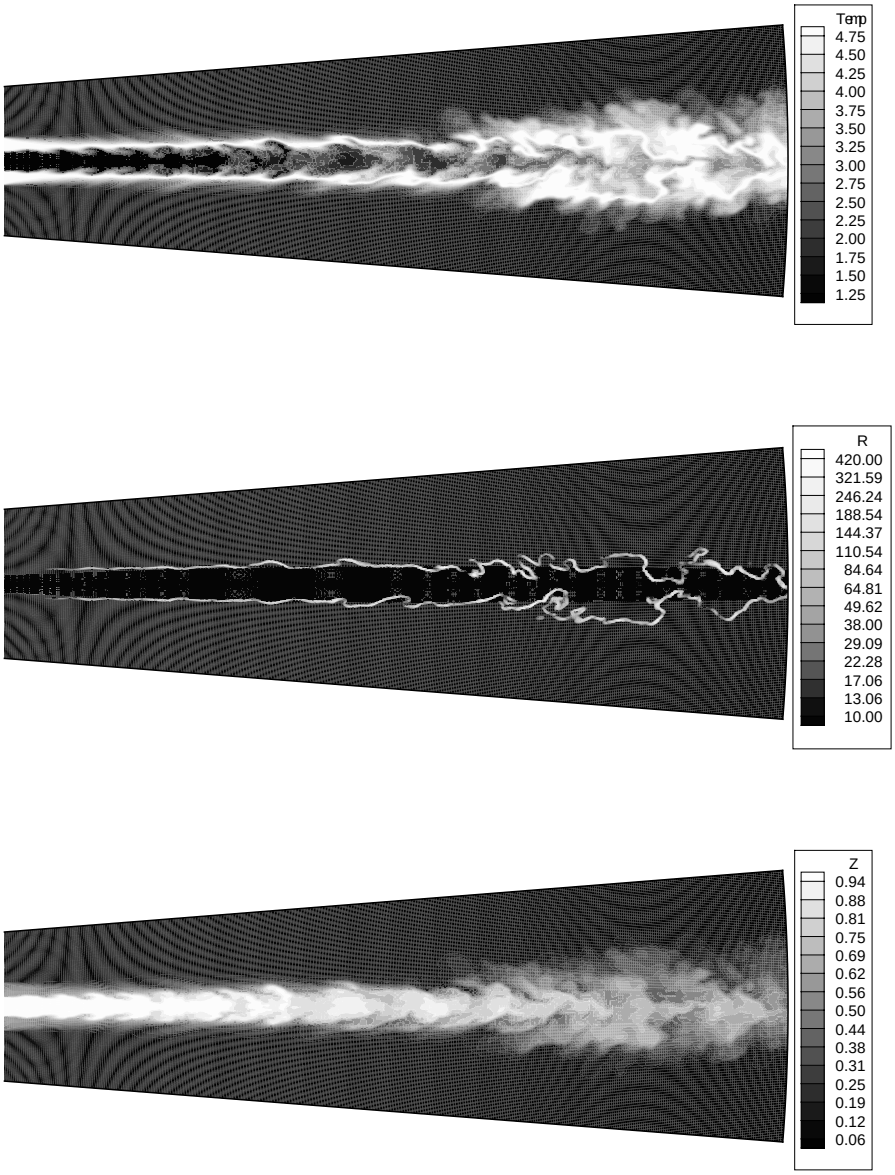

FIGURE 4. Top: The temperature distribution in the reacting jet; middle: The reaction rate in the turbulent jet; bottom: the mixture fraction Z as defined by Eq. (19).

pilot $Y_f = Y_o = 0.005$. The pre-exponential factor A is equal to 10^5, the Zeldovich number β equal to 8, and the heat release parameter α is equal to 0.8.

The reaction $F + O \rightarrow 2P$ is only an approximation to the chemistry occurring in real life. Even for a simple Hydrogen/Oxygen reaction, this is not a very good model, but it still allows us to study the interaction between heat-release and turbulence in a real three-dimensional flow. This can not be done with real chemistry because in this case all the intermediate species have to be stored in the computer

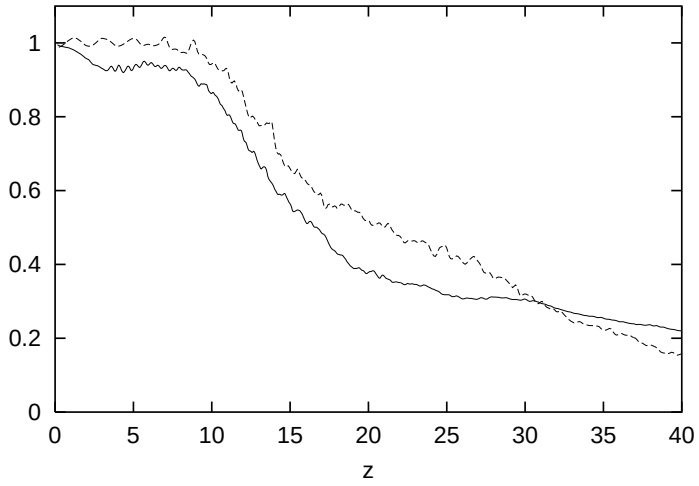

FIGURE 5. The centerline flux ρu_z as a function of the axial coordinate z. Non reacting jet: ——— ; reacting jet: - - - - .

memory and integrated, which is even with today's powerful parallel computers not really feasible for a full 3D calculation.

4. Results

In this section we will present some results obtained from the reacting jet simulations. The grid used in all the simulations consisted of $448 \times 80 \times 96$ points in the radial, tangential, and azimuthal direction respectively. The Reynolds number based on the cold orifice velocity and orifice diameter was equal to $4,000$. The calculations were run sufficiently long to be independent of the initial conditions. After reaching the steady state typically 60 independent data fields equally separated in time by $2D/U_{orifice}$ were stored for data analysis. All the statistics shown in this section have been calculated using the data from these 60 samples. In almost all studies dealing with jet flows, a cylindrical system is used; therefore, in the sequel of this paper, we will adopt such a system.

In Fig. 3 we show a typical snapshot of the fuel distribution in the heated jet (top), and in the lower figure we show a snapshot for a cold jet.

In the cold jet there is a clear Kelvin Helmholtz instability present close to the jet orifice. In the reacting case this instability is much weaker. This is mainly caused by dilatational effects in the flow and **not** by an increase viscosity. (This has been established by performing a simulation with constant viscosity and chemical heat release). Consequently, turbulent mixing in the heated jet is much smaller than in the cold jet.

In Fig. 4 we show the temperature distribution, the reaction rate (18), and the mixture fraction Z in the heated jet. The mixture fraction for the reaction (16) reads

$$Z = \frac{1}{2}\left(1 + Y_f - Y_o\right). \tag{19}$$

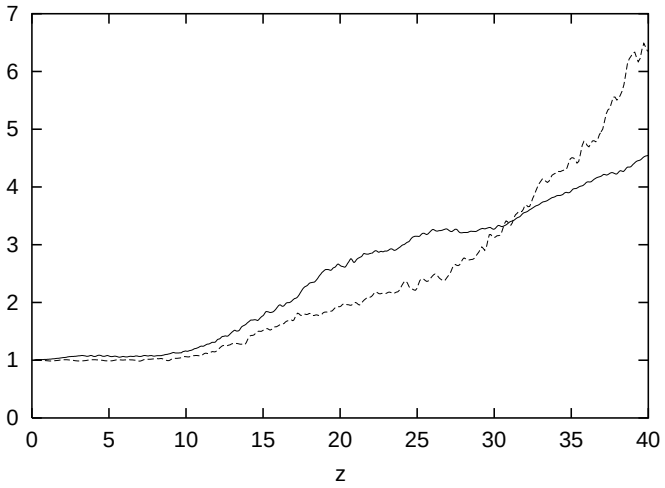

FIGURE 6. The inverse of the centerline flux $(\rho u_z)^{-1}$ as a function of the axial coordinate z. Non reacting jet: ——— ; reacting jet: - - - - .

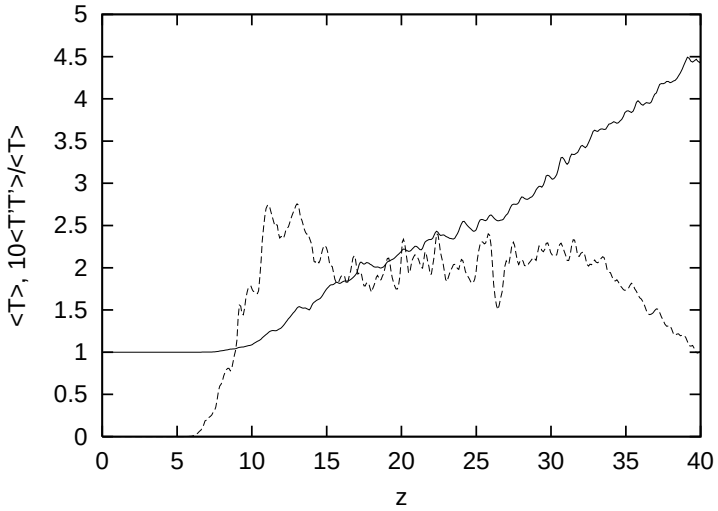

FIGURE 7. The centerline temperature as a function of the distance to the orifice. Non reacting jet: ——— ; reacting jet: - - - - .

Figure 5 shows that the transition to a turbulent flow occurs far downstream from the jet orifice compared to standard jets (Boersma *et. al*, 1997). This is due to the decreased mixing in the reacting jet, which delays the closing of the potential core and consequently the transition to a turbulent state. In the turbulent region mixing is high and, consequently, the temperature increases. Figure 4 (middle), in which the chemical source term given by Eq. (18) is plotted, shows that the region where the chemical reaction is occurring is very thin and strongly wrinkled in the turbulent region. The mixture fraction (Fig. 4, bottom) shows that there is not much mixing close to the jet orifice and that the flow is quite well mixed in the downstream region ($Z \approx 0.5$).

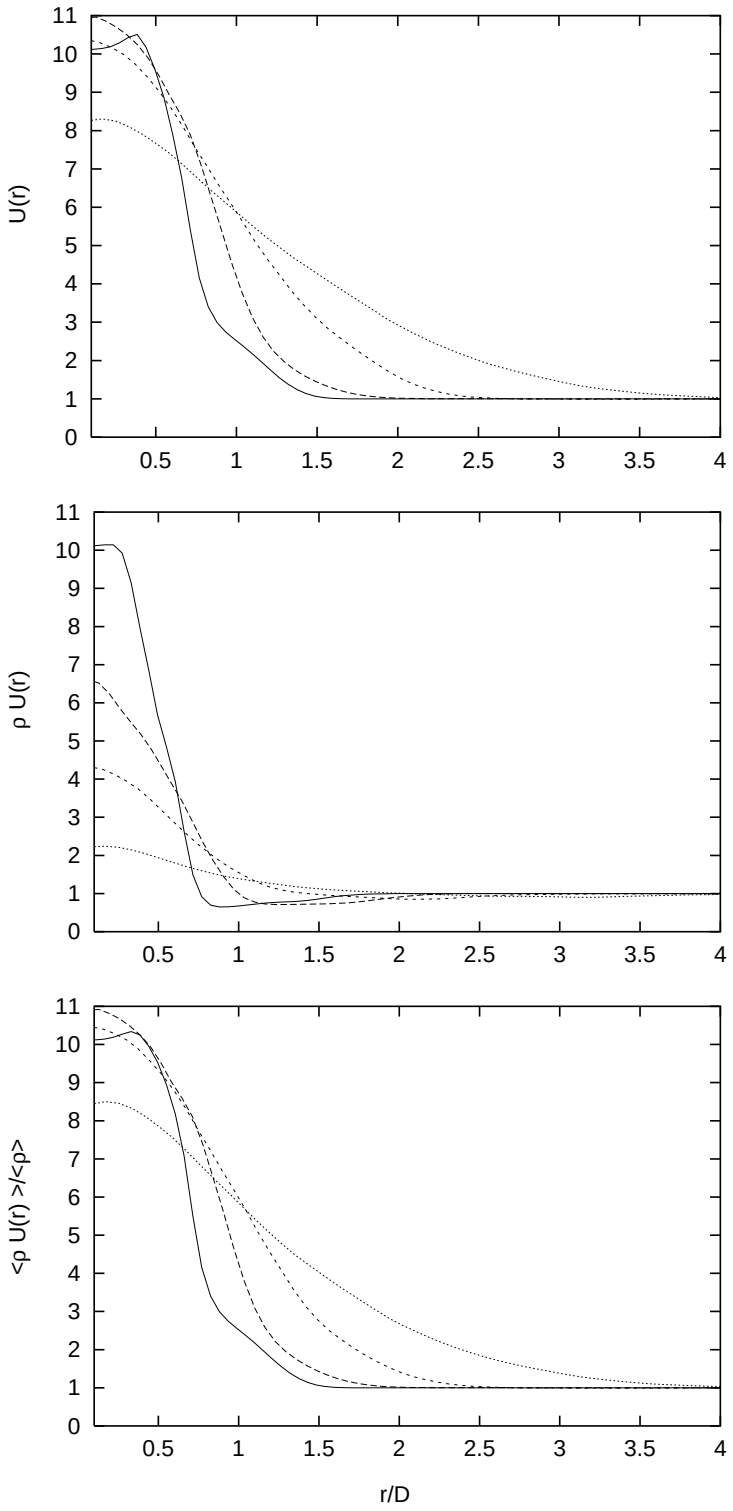

FIGURE 8. The mean axial velocity $U(r)$, axial flux $\rho U(r)$ and the Favre averaged velocity $\tilde{U}(r)$ as a function of the radial coordinate r at four different downstream locations. z=5D: ——— ; z=15D: — — — ; z=25D: - - - - ; z=35D:····· .

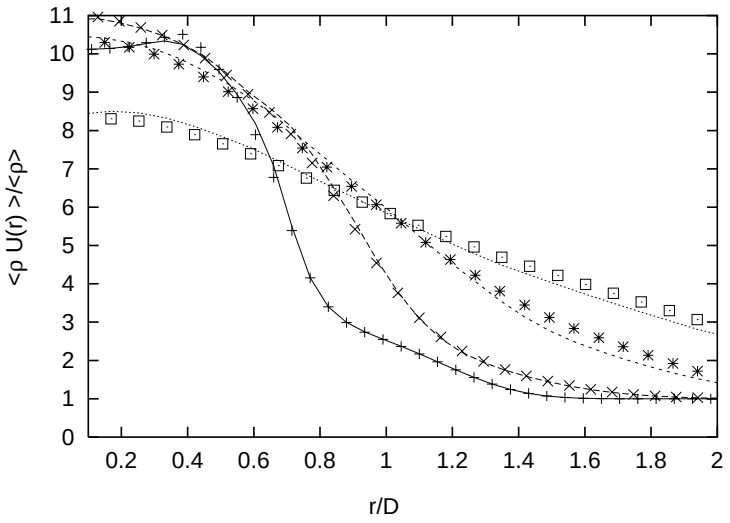

FIGURE 9. The axial velocity and Favre averaged axial velocity (symbols) at various downstream locations. z=5D: ——— ; z=15D: – – – ; z=25D: - - - - ; z=35D: ····· . z=5D: + ; z=15D: × ; z=25D: ∗ ; z=35D: □ .

Statistics

In this section some statistics which are obtained from the database are presented.

Figure 5 shows the axial flux ρu_z at the centerline as a function of the downstream distance for both a reacting and a non-reacting jet. For both jets the centerline velocity is more or less constant during the first 10 diameters and then drops quite rapidly.

In Fig. 6, the inverse of the axial flux $(\rho u_z)^{-1}$ is plotted as a function of the downstream distance for both the reacting and non-reacting jets. From this figure it can be seen that the decay of the cold jet is almost linear. For coflowing jets in contradiction to free jets, no real linear decay is expected from turbulence theory (see for instance Nickels & Perry 1996). The burning jet shows two different decay rates. The decay in the first 28 diameters is mainly due to diffusion and is, therefore, rather slow. At approximately $28D$ downstream of the orifice, the slope suddenly changes. This is the point where the the flow becomes truly turbulent (see Fig. 4), and due to enhanced mixing the decay rate of the jet changes.

In Fig. 7 the centerline jet temperature as a function of the distance to the jet orifice is shown. The centerline temperature shows a linear increase with the distance to the orifice, with again a change in slope around $z = 28D$. At the end of the computational domain, the centerline temperature still increases. However, it can never go above $T = T_b = 5$ because then all the fuel is burned and $\dot{\omega} = 0$. It seems that the computational domain is just a little bit too short to reach this temperature. In Fig. 7 the normalized rms of the temperature has been plotted as a function of the distance to the orifice. This rms value is more or less constant over the range $z = 12 - 32D$. For **cold** jets Dowling & Dimotakis (1990) report values of 0.23 for the normalized concentration rms in their $Re = 5000$ experiment. They claim that this value is not dependent on the axial coordinate. Surprisingly,

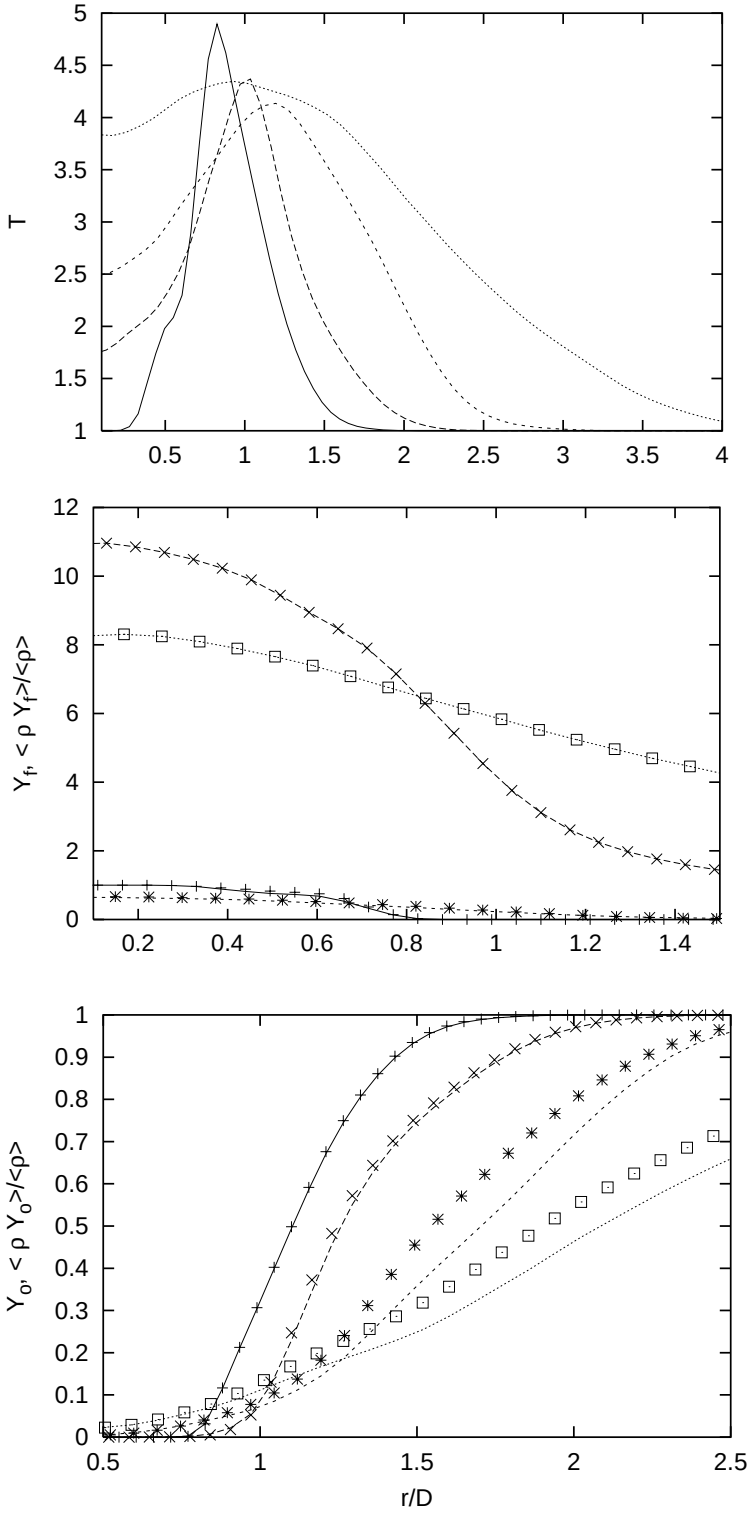

FIGURE 10. From top to bottom: The temperature, fuel concentration (non-Favre averaged and Favre averaged), oxidizer concentration (non Favre averaged and Favre averaged) at four downstream locations (Favre averaged results are plotted with symbols). z=5D: ——— ; z=15D: — — — ; z=25D: - - - - ; z=35D: ····· . z=5D: + ; z=15D: × ; z=25D: ∗ ; z=35D: □ .

even with a considerable decrease in the density, we find in the range $z = 12 - 30D$ a normalized rms value of 0.21, which is very close to the experiment.

In Fig. 8 the mean axial velocity profile, the axial flux ρu_z, and also the Favre averaged axial velocity

$$\tilde{u}_i = \frac{\overline{\rho u_i}}{\overline{\rho}}, \tag{20}$$

are shown. This Favre averaged velocity is of particular interest because, in most engineering models of compressible turbulence and combustion, the real velocity is replaced by its Favre averaged counterpart (Gatski, 1997). The advantage of this is that the term $\partial(\overline{\rho u_i})/\partial t$ can be replaced by $\partial(\overline{\rho}\tilde{u}_i)/\partial t$, where a bar can be a Reynolds average or a large eddy filter operator. For compressible flows the Favre averaging is in general a reasonable assumption because density variations are rather small and most times appear on larger scales than velocity fluctuations. However, for combustion, density ratios are by definition large, and it is not clear if it is justified to replace the unsteady term by the Favre average.

In Fig. 9 we show the axial velocity and the Favre averaged axial velocity in one figure, i.e Figs. 8a and 8c. At the locations close to the jet orifice ($z = 5D$ and $z = 15D$), there is no difference between the Favre averaged velocity and the regular velocity. At the other two downstream locations shown in Fig. 9, there are some very small differences. The Favre averaged velocities are in general a little bit lower close to the jet centerline and a bit larger for large radii. However, in general we can say that it seems justified to assume Favre averages for the velocity field.

To continue, we show in Fig. 10 the mean temperature, mean fuel concentration, and mean oxidizer concentration profiles, both Favre averaged and non Favre averaged (the Favre average for temperature is not shown because it is identical to the temperature since we assume ρT is constant.) The difference between Favre averaged mass fractions and the normal mass fractions is considerably larger than for the velocity profiles. This will have considerable implications for chemistry models using the Favre averaged equations.

6. Conclusion

In this paper we have presented some results obtained from a DNS of a reacting jet with considerable chemical heat release. It has been shown that, due to the chemical heat release, turbulent fluctuations are suppressed and that the transition to turbulence is delayed. Furthermore, it has been shown that there is a difference between the Favre and non-Favre averaged quantities close to the jet centerline. This is especially true for the chemical species. This implies that, in a model which solves for Favre averaged variables, the difference between the Favre averaged and normal variables should be taken into account or the modeling of Favre averaged quantities should be abandoned.

REFERENCES

Boersma, B. J., Brethouwer, G., & Nieuwstadt, F. T. M. 1998 A numerical investigation on the effect of the inflow conditions on the self-similar region of a round jet. *Phys of Fluids.* **10,** 899-909.

Boersma, B. J., & Lele, S. K. 1999 Large eddy simulation of Mach 0.9 compressible jet. *AIAA paper 99-1874.*

Chen, J. H., Mahalingam, S., Puri, K. I., & Vervisch, L. 1992 Effect of finite-rate chemistry and unequal Schmidt numbers on turbulent non-premixed flames modeled with single step chemistry. *Proceedings of the 1992 Summer Program,* Center for Turbulence Research, NASA/Stanford Univ. 367-387.

DesJardin, P. E., & Frankel, S. H. 1998 Large eddy simulation of a non-premixed reacting jet: Application and assessment of subgrid-scale combustion models. *Phys of Fluids.* **10,** 2298-2314.

Dowling, D. R., & Dimotakis, P. E. 1990 Similarity of the concentration field of gas-phase turbulent jets. *J. Fluid Mech.* **218,** 109-141.

Ferziger, J. H. 1996 Large eddy simulation: its role in turbulence research. In *Simulation and modeling of turbulent flows,* eds. T. B. Gadski, M. Y. Hussaini, and J. L. Lumley, Oxford University Press, New-York, 109-154.

Galperin, B., & Orszag, S. A. 1993 *Large eddy simulation of complex engineering and geophysical flows.* Cambridge Univ. Press, UK.

Gatski, T. B. 1997 Modeling of compressibility effect on turbulence, In: *New tools in turbulence modeling,* O. Metais and J. Ferziger, eds., Springer Verlag, Berlin.

Gear, C. W. 1971 *Numerical initial value problems in ordinary differential equations.* Prentice Hall, New Jersey.

Koren B. 1993 A robust upwind discretization method for advection, diffusion and source terms. In *Numerical methods for advection-diffusion problems*, eds. Vreugdenhill, C. B., Koren, B., Notes on Numerical Fluid Mechanics, Vieweg-Braunschweig. *45.* **117-138.**

Lubbers, C. L., Brethouwer, G., Boersma, B. J., & Nieuwstadt, F. T. M. 1999 Simulation of the mixing of a passive scalar in a round turbulent jet. Submitted to *Fluid Dynamics Research.*

McMurtry, P. A., Jou, W. H., Riley, J. J., & Metcalfe, R. W. 1986 Direct numerical simulations of a reacting mixing layer with chemical heat release. *AIAA J.* **24,** 962-970.

Moin, P., & Mahesh, K. 1998 Direct numerical simulation: A tool in turbulence research. *Ann. Review Fluid Mech.* **30,** 539-578.

Najm, H. N., Wyckoff, P. S., & Knio, O. M. 1998 A semi-implicit numerical scheme for reacting flow. *J. of Comp. Phys.* **143,** 381-402.

Nickels, T. B. & Perry, A. E. 1996 An experimental and theoretical study of the turbulent coflowing jet. *J. Fluid Mech.* **309,** 157-183.

Rutland, C. J., Ferziger, J. H., & Cantwell, B. J. 1989 Effects of strain, vorticity, and turbulence on premixed flames. *Report TF-44.* Stanford University, Stanford CA.

Vervisch, L., & Poinsot, T. 1998 Direct numerical simulation of non-premixed turbulent flames. *Ann. Rev. Fluid Mech.* **30,** 655-691.

Wall, C., Boersma, B. J., & Moin, P. 1999 An evaluation of the assumed beta PDF subgrid scale model for LES of non-premixed turbulent combustion with heat release. Submitted to *Phys of Fluids.*